

## ORIGINAL ARTICLE

# Compositional control of radionuclide retention in hollandite-based ceramic waste forms for Cs-immobilization

Mingyang Zhao<sup>1</sup> | Yun Xu<sup>1</sup> | Lindsay Shuller-Nickles<sup>2,3</sup> | Jake Amoroso<sup>4</sup> | Anatoly I. Frenkel<sup>5,6</sup> | Yuanyuan Li<sup>5</sup> | Weiping Gong<sup>7</sup> | Kristina Lilova<sup>7</sup> | Alexandra Navrotsky<sup>7</sup>  | Kyle S. Brinkman<sup>1,3</sup> 

<sup>1</sup>Department of Materials Science and Engineering, Clemson, South Carolina

<sup>2</sup>Department of Environmental Engineering and Earth Sciences, Clemson, South Carolina

<sup>3</sup>Center for Nuclear Environmental Engineering Sciences and Radioactive Waste Management (NEESRWM), Clemson University, Clemson, South Carolina

<sup>4</sup>Savannah River National Laboratory, Aiken, South Carolina

<sup>5</sup>Department of Materials Science and Chemical Engineering, Stony Brook University, Stony Brook, New York

<sup>6</sup>Division of Chemistry, Brookhaven National Laboratory, Upton, New York

<sup>7</sup>Peter A. Rock Thermochemistry Laboratory and NEAT ORU, University of California Davis, Davis, Carolina

## Correspondence

Kyle S. Brinkman, Department of Materials Science and Engineering, Clemson, SC.

Email: ksbrink@clemson.edu

## Funding information

US Department of Energy, Grant/Award Number: DE- SC0012530, DE-FG02-03ER15476, DE-SC0001089, DE-SC0016574, DE-AC09-08SR22470; U.S. Department of Energy

## Abstract

Hollandite materials, as a class of crystalline nuclear waste forms, are promising candidates for the immobilization of radioactive elements, such as Cs, Ba, as well as a variety of lanthanide and transition-metal fission products. In this study, three Ga-doped titanate hollandite-type phases,  $\text{Ba}_{1.33}\text{Ga}_{2.67}\text{Ti}_{5.33}\text{O}_{16}$ ,  $\text{Ba}_{0.667}\text{Cs}_{0.667}\text{Ga}_2\text{Ti}_6\text{O}_{16}$ , and  $\text{Cs}_{1.33}\text{Ga}_{1.33}\text{Ti}_{6.67}\text{O}_{16}$ , were synthesized using a solid-state reaction route. All synthesized phases adopted a single phase tetragonal structure, as determined by powder X-ray diffraction (XRD), and elemental analysis confirmed the measured stoichiometries were close to targeted compositions. Extended X-ray absorption fine structure spectroscopy (EXAFS) was used to determine the local structural features for the framework of octahedrally coordinated cations. EXAFS data indicated that  $\text{Cs}_{1.33}\text{Ga}_{1.33}\text{Ti}_{6.67}\text{O}_{16}$  possessed the most disordered local structure centered around the Ga dopant. The enthalpies of formation of all three hollandite phases measured using high-temperature oxide melt solution calorimetry were found to be negative, indicating enthalpies of formation of these hollandites from oxides are thermodynamically stable with respect to their constituent oxides. Furthermore, the formation enthalpies were more negative and hence more favorable with increased Cs content. Finally, aqueous leaching tests revealed that high Cs content hollandite phases exhibited greater Cs retention as compared to low Cs content hollandite. While preliminary in nature, this work draws attention to the links between the capacity for radionuclide retention, atomistic level structural features and bulk thermodynamic properties of materials.

## 1 | INTRODUCTION

Suitable materials are needed to sequester waste products resulting from potential commercial nuclear fuel recycling and to treat existing waste resulting from decades of reactor operation for power production.<sup>1</sup> Moreover, advanced

waste form materials are needed to reduce the environmental and financial impacts of nuclear power generation, which are inextricably linked to ultimate disposition of the waste products.<sup>2</sup> Borosilicate glass is the most universally accepted and produced nuclear waste form to immobilize both defense and commercial waste products.<sup>3</sup> However,

phase separation or crystallization of borosilicate glass commonly happen even at low waste loading due to limited solubility of some specific fission products, which motivates the development of alternative waste forms with improved performance and properties for nuclear waste immobilization and disposition.<sup>4,5</sup>

Synthetic rock (SYNROC), first proposed in the 1970s, is a polycrystalline waste form engineered to sequester various waste elements in specific crystalline lattice sites.<sup>6–8</sup> Typical constituent phases of SYNROC such as perovskite, hollandite, and zirconolite phases have been demonstrated to accommodate a wide range of radionuclides and non-radioactive species in high-level waste (HLW) such as corrosion products resulting from the removal and dissolution of hulls and hardware.<sup>9</sup> Among the SYNROC crystalline phases, hollandite-type structures are designed to immobilize alkali and alkaline-earth elements, including Cs and its beta-decay product Ba.<sup>9</sup>

The general chemical formula of these hollandite-type materials can be written as  $A^{+2+}_x B^{2+/3+/4+}_8 O_{16}$  ( $0 < x < 2$ ), where A-sites are usually occupied by alkali and/or alkaline-earth elements (eg, Na, K, Rb, Cs, Sr, and Ba) and B-sites are often occupied by a variety of cations (eg, Mg, Co, Ni, Zn, Al, Ga, Cr, Fe, Ti, and Mn).<sup>9–12</sup> Hollandites have been studied for a variety of applications, such as oxygen evolution reaction catalysts ( $K_{x \approx 2} Ir_8 O_{16}$ ), ferromagnetic materials ( $Ba_{1.2} Mn_8 O_{16}$ ), and battery electrode systems with  $M_x Mn_8 O_{16}$  ( $M = Ag$  or  $K$ ) demonstrated as cathodes, and  $K_2(M_2 Sn_6) O_{16}$  ( $M = Co, In$ ) used as anode materials.<sup>13–17</sup> In SYNROC-based materials for nuclear waste immobilization, the multiphase system is based on thermodynamically compatible titanate phases. For the hollandite phase, this results in  $Ti^{4+}$  as the major B-site cation. Although many compositions and potential B-site dopants exist, current strategies for waste form processing based on

melting and crystallization require temperatures in excess of  $1400^\circ C$ , which poses potential processing limitations and increased volatilization of species such as Ba and Cs.<sup>5</sup> Two prominent advantages of using gallium in the hollandite B-site are that Ga has potentials to lower the melting point of hollandite compared with traditional Al- and Cr-doped hollandites and that Ga has demonstrated redox stability in a range of oxygen activity conditions encountered in high-temperature melt processing.<sup>12,18,19</sup> Therefore, this study is focused on titanate-based hollandite of the form  $Ba_x Cs_{1.33-x} Ga_{1.33+x} Ti_{6.67-x} O_{16}$  ( $x = 0, 0.667, 1.33$ ) with  $Ga^{3+}$  partially substituted on Ti sites.

The idealized titanate-based hollandite structure is graphically depicted in Figure 1. A  $2 \times 2$  tunnel is created by eight edge and corner sharing octahedra consisting of metal cations (Ga and Ti) on B-sites and coordinated oxygen anions, while cations on A-sites (Ba and Cs) are immobilized inside the tunnel. Depending on the radius ratio of A-site to B-site cations, hollandites may adopt two distinct crystal structures: tetragonal ( $I4/m$ ) and monoclinic ( $I2/m$ ) phases.<sup>20</sup> Several studies have been reported on the mobility and ordering of A-site tunnel cations in hollandite-type systems while evaluating their potential as fast-ion conductors in battery systems.<sup>21,22</sup> However, there are limited reported studies on the ordering of B-site framework cations in hollandite structures.<sup>23</sup> The local structure and short-range order are expected to significantly impact the physical properties of these materials, and a better understanding of the atomic-scale structure is needed to optimize hollandite-type phases for use as waste forms. Moreover, the structure, thermodynamic stability, and propensity for radionuclide retention in these materials are surely related, and an improved understanding of the former will undoubtedly lead to a more enlightened design of materials for nuclear waste immobilization.

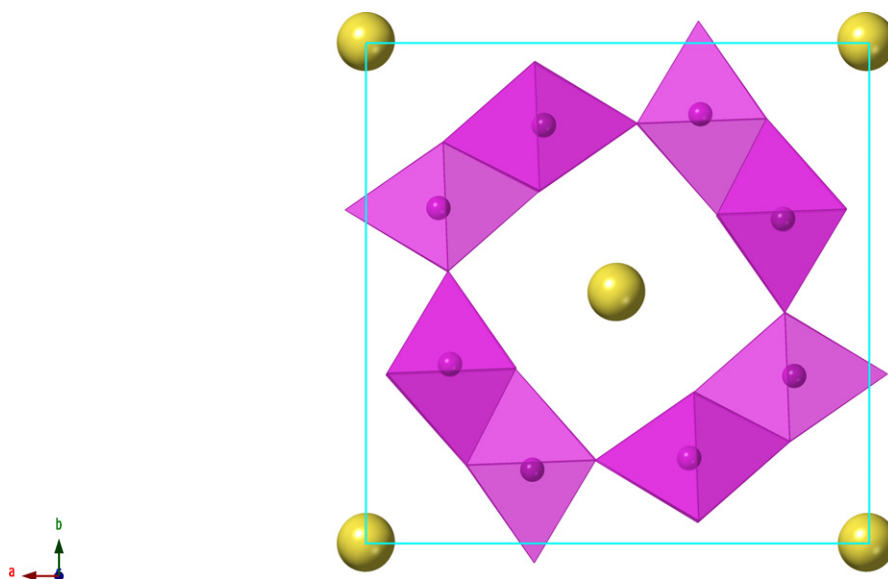


**FIGURE 1** Two-dimensional [0 0 1] projection of titanate base hollandite structure. Yellow balls represent cations on A-sites, purple balls represent  $Ti^{4+}$ /metal cations (M) on B-sites, purple octahedra represent  $[(Ti^{4+}, M)O_6]$  units, and blue lines outline the unit cell. Here, oxygen atoms composing the octahedra are omitted for simplification

In this study, the links between the atomic-level local structure of framework cations, thermodynamic stability, and elemental release performance of a series of Ga-doped titanate hollandite phases are reported for the first time using advanced characterization techniques including extended X-ray absorption fine structure (EXAFS), high-temperature oxide melt solution calorimetry and powder-based leach testing.

## 2 | MATERIALS AND METHODS

### 2.1 | Sample synthesis

Three Ga-doped titanate hollandite samples with chemical formula  $\text{Ba}_x\text{Cs}_{1.33-x}\text{Ga}_{1.33+x}\text{Ti}_{6.67-x}\text{O}_{16}$  ( $x = 0, 0.667, 1.33$ ) were synthesized via a solid-state reaction route. They are denoted as  $\text{Ba}_{1.33}\text{Ga}_{2.67}$ ,  $(\text{BaCs})_{0.667}\text{Ga}_2$ ,  $\text{Cs}_{1.33}\text{Ga}_{1.33}$ , respectively, in following text for simplicity. An additional hollandite composition with chemical formula  $\text{Ba}_{1.04}\text{Cs}_{0.24}\text{Ga}_{2.32}\text{Ti}_{5.68}\text{O}_{16}$  was prepared using solid-state reaction which is denoted as  $\text{Ba}_{1.04}\text{Cs}_{0.24}\text{Ga}_{2.32}$ . This composition was selected to match the Cs content for the majority of hollandite literature and to provide additional data for Cs-dependent elemental release studies.

Reagent-grade powders of barium carbonate,  $\text{BaCO}_3$  (99.98%; Sigma-Aldrich, St. Louis, MO), cesium carbonate,  $\text{Cs}_2\text{CO}_3$  (99.9%; Alfa Aesar, Haverhill, MA, USA), gallium oxide,  $\text{Ga}_2\text{O}_3$  (99.99%; Sigma-Aldrich) and titanium oxide (anatase),  $\text{TiO}_2$  (99.8%; Sigma-Aldrich), were used as starting materials without further purification. Stoichiometric mixtures of raw powders were added into high-density polyethylene (HDPE) jars to make five-gram batches, followed by mixing with ethanol and ball-milling for 24 hours, and finally drying in an oven. As-dried powders were ground in an agate mortar/pestle and cold-pressed into pellets. Heat-treatment processes, including calcination and sintering, were performed in a box furnace (Lindberg). Samples were prepared as follows: (a)  $(\text{BaCs})_{0.667}\text{Ga}_2$  and  $\text{Cs}_{1.33}\text{Ga}_{1.33}$  samples were calcined in air for 10 hours at  $1200^\circ\text{C}$ , followed by sintering in air for 3 hours at  $1250^\circ\text{C}$ ; (b)  $\text{Ba}_{1.33}\text{Ga}_{2.67}$  samples were calcined at  $1250^\circ\text{C}$  for 5 hours and sintered at  $1275^\circ\text{C}$  for 3 hours; (c) finally, an intermediate composition  $\text{Ba}_{1.04}\text{Cs}_{0.24}\text{Ga}_{2.32}\text{Ti}_{5.68}\text{O}_{16}$  ( $\text{Ba}_{1.04}\text{Cs}_{0.24}\text{Ga}_{2.32}$ ) was prepared by calcining at  $1150^\circ\text{C}$  for 30 hours and sintering at  $1250^\circ\text{C}$  for 3 hours.<sup>12\*</sup> This composition was selected to match the Cs content for the majority of hollandite literature and to provide additional data for Cs-dependent elemental release studies. To reduce the vaporization of Cs and Ba at elevated temperature

during sintering, crucibles were covered with alumina lids and sealed with cement (Aremco Products, Valley Cottage, NY) and the pellets were immersed and covered with additional calcined powders.

### 2.2 | Characterization

Powder X-ray diffraction (XRD) measurements of crystal structures of three hollandite phases were conducted by Rigaku Ultima IV diffractometer with monochromatic  $\text{Cu K}\alpha$  radiation ( $\lambda = 1.54 \text{ \AA}$ ). The data were collected from  $20$  to  $70^\circ 2\theta$  with a  $0.02^\circ$  step size at  $40 \text{ kV}$  and  $200 \text{ mA}$ . The microstructure and chemical composition of sintered samples were investigated by a Hitachi SU6600 scanning electron microscopy (SEM; Hitachi, Tokyo, Japan) equipped with energy dispersive X-ray spectroscopy (EDS) analysis (Oxford, Buckinghamshire, UK). It is noted that samples were not polished and coated prior to EDS measurements, to avoid introduction of impurities. The EDS composition is reported as the average of the composition of eight to thirteen different sites over the representative sample cross-sectional surface. Inductively coupled plasma-mass spectroscopy (ICP-MS) was used to measure Cs concentrations, and inductively coupled plasma-atomic emission spectroscopy (ICP-AES) was used to measure Ba, Ga, and Ti concentrations. A lithium metaborate (LM) fusion preparation with nitric acid digestion was used to dissolve solid samples for ICP-MS and ICP-AES analysis. Back-scattered electron (BSE) imaging mode was selected to observe the morphology of sintered pellets. EXAFS spectra were collected for the well-ground samples at Stanford Synchrotron Radiation Lightsource (SSRL) beamline 2-3 in a transmission mode. The spectra were calibrated by gallium foils and all data were collected at room temperature. Raw data were processed with the Athena software.<sup>24</sup> The Fourier transform to the  $R$ -space was taken in the  $k$  range  $2$ – $13 \text{ \AA}^{-1}$  by Fourier transforming  $k^3\chi(k)$  with Hanning window. Curve fitting was performed with the Artemis and IFEFFIT software using ab initio-calculated phases and amplitudes from the program FEFF 8.2.<sup>24</sup> The goodness-of-fit was determined by the residual component  $R$ . Structural data from previously reported density functional theory (DFT) calculations was further analyzed and compared with EXAFS measurements.<sup>23</sup>

### 2.3 | High-temperature oxide melt solution calorimetry

High-temperature oxide melt solution calorimetry was performed using a custom-built Tian-Calvet twin calorimeter operating at  $702^\circ\text{C}$ . In a drop solution calorimetry experiment approximately  $5 \text{ mg}$  weighed samples were loosely pressed into pellets and dropped from room temperature

\*The processing conditions have been optimized to reduce Cs loss and enhance phase purity, the calcination and sintering temperatures utilized in this work are different from prior works.<sup>12,30</sup>

into the molten solvent (sodium molybdate:  $3\text{Na}_2\text{O} \cdot 4\text{MoO}_3$ ) in a platinum crucible in the calorimeter. Detailed instrument and experimental procedure can be found by Navrotsky.<sup>25,26</sup> To stir the melt and improve the rate of dissolution of pellets, the calorimeter assembly was flushed with oxygen gas at 43 mL/min and oxygen gas was bubbled through the solvent at 4 mL/min. At least eight successful drops were performed for each composition to obtain statistically reliable data. The calorimeter was calibrated utilizing the heat content of  $\alpha$ -alumina. This methodology is well-established and has been described previously.<sup>25,26</sup>

## 2.4 | Leaching test

A crushed sample leaching test following guidelines in the Product Consistency Test (PCT; Method-B) was performed on each sample to assess aqueous chemical durability.<sup>27,28†</sup> For each hollandite composition, three PCT samples were prepared. Two different particle sizes (sieve fractions  $-100/+200$  and  $-200/+270$  mesh) were prepared for each composition. Assuming all particles are spherical, the  $-100/+200$  and  $-200/+270$  sieve fraction had an average particle diameter ( $D$ ) of 112.5 and 64  $\mu\text{m}$ , respectively. The density of hollandite samples was estimated as 4.8  $\text{g}/\text{cm}^3$ . A standard material referred to as the approved reference material (ARM) was measured in triplicate along with the sample matrix. A single particle size (sieve fraction  $-100/+200$  mesh) was used for all three ARM samples. Each sample and the ARM standard were ground, washed with water, and prepared following the standard PCT procedure.<sup>27</sup> A ratio of 10 mL water to 1 g sample or standard was combined in stainless steel vessels. The vessels were closed, sealed, and placed in an oven at  $90 \pm 2^\circ\text{C}$ ; the samples were maintained at this temperature for 7 days. Once cooled, the resulting solutions were sampled (filtered and acidified) and analyzed. The normalized elemental release ( $NL_i$ ) was calculated using the Equation (1):

$$NL_i = \frac{C_i}{f_i \times SA/V} \quad (1)$$

where  $NL_i$  = normalized elemental release ( $\text{g}/\text{m}^2$ ),  $C_i$  = concentration of element “i” (eg, Cs) in the leachate solution ( $\text{g}/\text{L}$ ),  $f_i$  = fraction of element “i” in the unleached waste form (unitless), and  $SA$  = surface area of the final waste form ( $\text{m}^2$ ),  $V$  = volume of leachant solution (L).<sup>‡</sup>

<sup>†</sup>The PCT has been used in ceramic waste form research as a convenient method to compare elemental releases within a sample matrix of controlled variables (ie, surface area) and identify phases with low durability. The test is not being used to provide quantitative durability values.

<sup>‡</sup>In the analysis,  $f_i$  represents the measured concentration, not the target composition.

Surface areas ( $SA$ ) were calculated based on the estimated density of the hollandite samples, the average particle size of each particle, and the total number of particles in the samples with a given mass. Additionally, as a method for comparison to other reported leach values in this system, fractional elemental release from the samples was calculated using the equation:

$$FR_i = \frac{C_i \times V}{m_s \times f_i} \quad (2)$$

where  $FR_i$  = fractional elemental release (unitless),  $C_i$  = concentration of element “i” (eg, Cs) in the leachate solution ( $\text{g}/\text{L}$ ),  $V_s$  = volume of leachant solution (L),  $m_s$  = mass (g) of sample, and  $f_i$  = fraction of element “i” in the unleached waste form (unitless). From Equation (2), the fractional elemental release ( $FR_i$ ) is obtained and used to facilitate a comparison of the relative release among the samples.

## 3 | RESULTS AND DISCUSSION

### 3.1 | Crystallographic and elemental analysis

Based on the XRD pattern of the reference material  $(\text{Cs}_{0.40}\text{Ba}_{0.79})(\text{Ti}_{1.99}\text{Ti}_{6.01})\text{O}_{16}$  (PDF#80-2269, tetragonal, space group:  $I4/m$ ), it was confirmed that all three hollandite phases were single phase and exhibited tetragonal

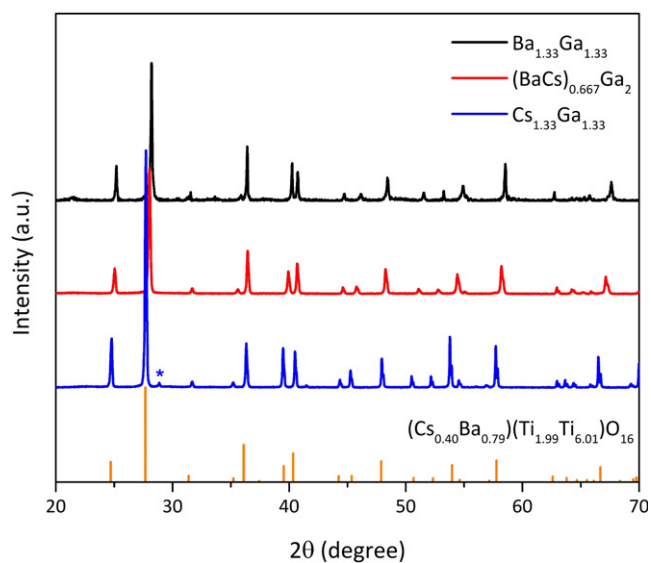


**FIGURE 2** XRD patterns of as calcined powders of three hollandite phases containing different Cs contents with fixed occupancy on A-sites. \*Indicates the titanium-rich secondary phase detected. Reference spectra for  $(\text{Cs}_{0.40}\text{Ba}_{0.79})(\text{Ti}_{1.99}\text{Ti}_{6.01})\text{O}_{16}$  (PDF#80-2269, tetragonal, space group:  $I4/m$ )

**TABLE 1** Target and analyzed compositions of sintered hollandite structured pellets based on SEM-EDS characterization, ICP-AES and ICP-MS<sup>a</sup>

Short name	Ga:Ti	Target composition	EDS composition	ICP composition
Ba <sub>1.33</sub> Ga <sub>2.67</sub>	1:2	Ba <sub>1.33</sub> Ga <sub>2.67</sub> Ti <sub>5.33</sub> O <sub>16</sub>	Ba <sub>1.27</sub> Ga <sub>2.71</sub> Ti <sub>5.33</sub> O <sub>16</sub>	Ba <sub>1.31</sub> Ga <sub>2.69</sub> Ti <sub>5.33</sub> O <sub>16</sub>
(BaCs) <sub>0.667</sub> Ga <sub>2</sub>	1:3	Ba <sub>0.667</sub> Cs <sub>0.667</sub> Ga <sub>2</sub> Ti <sub>6</sub> O <sub>16</sub>	Ba <sub>0.62</sub> Cs <sub>0.62</sub> Ga <sub>2.05</sub> Ti <sub>6</sub> O <sub>16</sub>	Ba <sub>0.67</sub> Cs <sub>0.53</sub> Ga <sub>2.04</sub> Ti <sub>6</sub> O <sub>16</sub>
Cs <sub>1.33</sub> Ga <sub>1.33</sub>	1:5	Cs <sub>1.33</sub> Ga <sub>1.33</sub> Ti <sub>6.67</sub> O <sub>16</sub>	Cs <sub>1.31</sub> Ga <sub>1.34</sub> Ti <sub>6.67</sub> O <sub>16</sub>	Cs <sub>1.16</sub> Ga <sub>1.39</sub> Ti <sub>6.67</sub> O <sub>16</sub>

<sup>a</sup>Compositions were normalized to Ti and oxygen contents were corrected to achieve charge balance.

symmetry (*I4/m*), with the exception of a weak peak of unknown secondary phase near 29° 2θ in the Cs<sub>1.33</sub>Ga<sub>1.33</sub> sample as indicated by the bold asterisk in Figure 2. This peak was ascribed to a residual Ti-rich phase due to vaporization of Cs, which was observed by X-ray absorption and electron probe micro-analysis according to previous studies.<sup>12,29</sup>

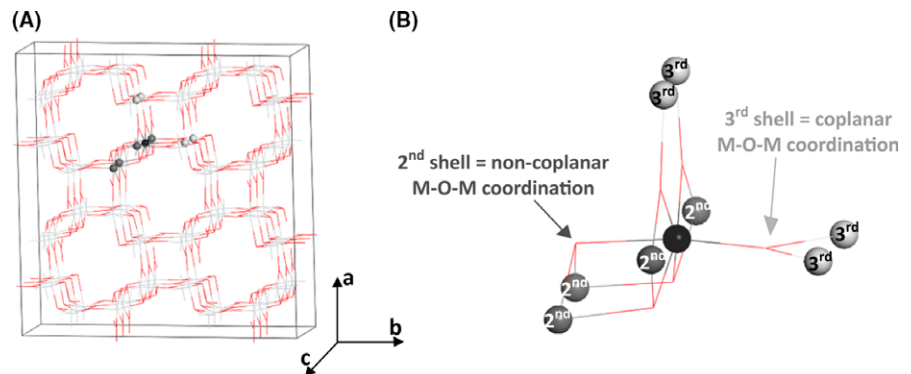
The elemental concentrations of Ba, Cs, Ga, and Ti of the synthesized materials were measured by EDS, ICP-AES, and ICP-MS analyses (Table 1). The EDS composition is reported as the average of the composition of eight to thirteen different sites over the representative sample cross-sectional surface. The EDS site map and elemental energy dispersive maps on Site 1, 3, and 7 of the Cs<sub>1.33</sub>Ga<sub>1.33</sub> sample serve as examples to illustrate the method in Figure S1. Figure S2 displays the BSE images of the sample surfaces of (a) Ba<sub>1.33</sub>Ga<sub>2.67</sub>, (b) (BaCs)<sub>0.667</sub>Ga<sub>2</sub>, and (c) Cs<sub>1.33</sub>Ga<sub>1.33</sub>. Although the EDS composition on Site 7 of the Cs<sub>1.33</sub>Ga<sub>1.33</sub> sample in Figure S1 (d) shows a representative “Ti-rich” area which is noted on the previous XRD patterns, BSE images in Figure S2 revealed no distinct phase segregation or secondary phases. The results generally confirm that targeted stoichiometries were acquired for all three hollandite phases. The actual compositions as determined by EDS, ICP-AES and ICP-MS analyses were used to calculate enthalpies of formation of all three hollandite phases. In addition, the microstructure generally followed prior observations with higher Cs loading compositions exhibiting a larger rod-like grain structure.<sup>12</sup>

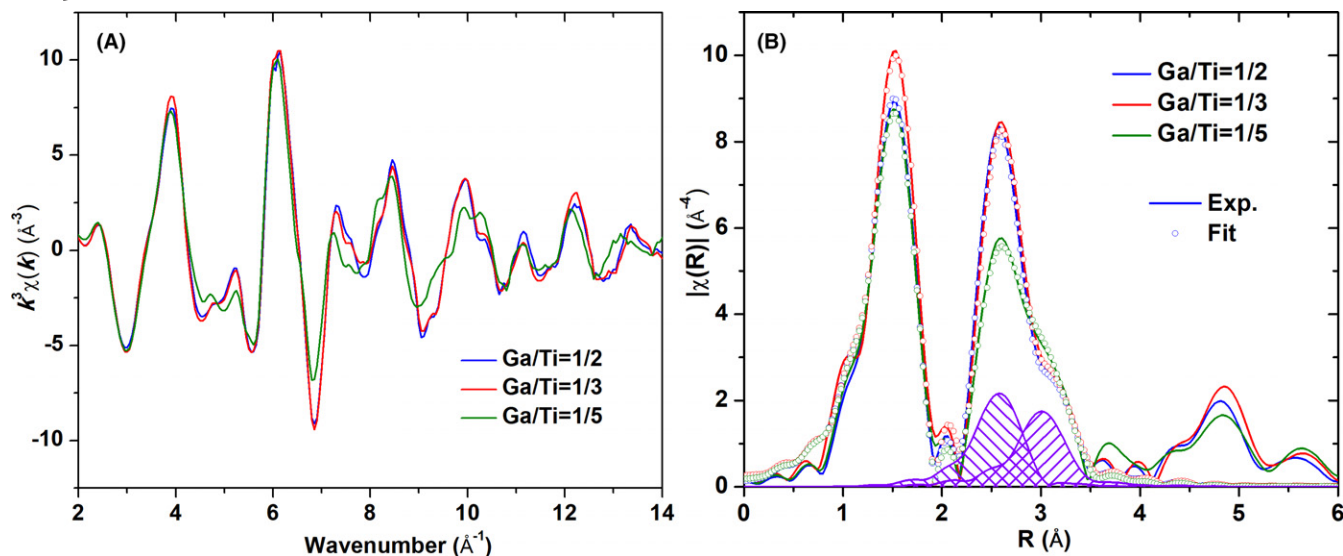
### 3.2 | EXAFS analysis

Figure 3A shows the crystal structure of hollandite along the *c*-axis (ie, the tunnel direction). The A-site cations are removed for clarity. Each B-site cation is coordinated with six O as the first shell, four metal cations as the second shell and four metal cations as the third shell in Figure 3B. Of note, the second shell M (Cation)-M (Cation) distances are connected via O1-type atoms, which may limit ion mobility along the tunnel.<sup>12,30</sup> The local structures around Ga for all three Ga-doped hollandite phases Ba<sub>1.33</sub>Ga<sub>2.67</sub>, (BaCs)<sub>0.667</sub>Ga<sub>2</sub> and Cs<sub>1.33</sub>Ga<sub>1.33</sub> with correspondingly different ratios of Ga:Ti (=1:2, 1:3, and 1:5) were examined by EXAFS. As shown in Figure 4A, the *k*-space spectra of the 1:2 and 1:3 ratio of Ga:Ti are very similar but are different from that of the 1:5 ratio of Ga:Ti, especially in the *k* range of 7-11 Å<sup>-1</sup>. Correspondingly, in *R*-space, the spectrum of the 1:5 ratio of Ga:Ti shows the lowest peak at the distance approximately 2.6 Å and the higher shoulder peak at about 3.2 Å in Figure 4B (no phase correction was used). As demonstrated in Figure 3B, these two patterned peaks in Figure 4B are due to different Ga-M distances in the second and third shells.

Extended X-ray absorption fine structure spectroscopy analysis was performed to (a) determine the types of elements in the second and third shell surrounding the centered Ga, and (b) obtain quantitative local structural information of the nearest environment around the centered Ga (ie, Ga-O coordination). Several models with six Ga-O bonds per Ga in the first shell but different degree of Ga-

**FIGURE 3** (A) Crystal structure of the lowest energy (BaCs)<sub>0.667</sub>Ga<sub>2</sub> hollandite configuration from DFT calculations looking along the tunnel direction (A-site cations removed for clarity). The second and third shells (B) of the B-site cations are highlighted





**FIGURE 4** (A)  $k^3$ -weighted EXAFS spectra  $\chi(k)$  and (B) their Fourier transform magnitudes for Ga K edge for three Ga-doped hollandite phases  $\text{Ba}_{1.33}\text{Ga}_{2.67}$ ,  $(\text{BaCs})_{0.667}\text{Ga}_2$  and  $\text{Cs}_{1.33}\text{Ga}_{1.33}$  with different ratios of Ga:Ti = 1:2, 1:3, and 1:5. The spectra obtained from EXAFS data fitting (circle) were also plotted to show the agreement between experimental data (solid line) and best-fit results. In addition, the peaks filled with patterns in the region of 2.0-3.5 Å indicate the contributions due to the second and third nearest Ga-M interactions. The two purple peaks were obtained by fitting the 1:5 ratio of Ga:Ti and the magnitude was reduced by 50% for better visualization

M interaction distances in the second and third shells were tested. Those models included: (a) four Ti in the second shell and four Ti in the third shell, (b) four Ga in the second shell and four Ga in the third shell, (c) four Ti in the second shell and four Ga in the third shell, (d) four Ga in the second shell and four Ti in the third shell, and (e) the total of four Ga and Ti in the second shell, and the total of four Ga and Ti in the third shell. In the latter case, the ratio of Ga:Ti in each shell was chosen according to the composition. Schematics for each of the possible second and third shell configurations for the EXAFS fittings are highlighted in Figure S3. Data for all three hollandites were fitted simultaneously within one global fitting procedure and the amplitude reduction factor ( $S_0^2$ ) was constrained to be the same for all compositions. The fitting  $k$  range was 2.5-12 Å<sup>-1</sup> and  $R$  range was 1.0-3.5 Å, and they were kept the same in testing different models. According to the fitting results, the model with four Ti in the second shell and four Ti in the third shell provided the best fitting and the most physically reasonable values of the fitting parameters. Physically, this corresponds to a larger probability of Ga-Ti as the nearest neighbors as opposed to Ga-Ga. The fitting results are listed in Table 2. DFT calculations from a recent study were further evaluated to consider the Ga-M interactions in the second and third shells for the lowest energy configurations for  $\text{Ba}_{1.33}\text{Ga}_{2.67}$ ,  $(\text{BaCs})_{0.667}\text{Ga}_2$  and  $\text{Cs}_{1.33}\text{Ga}_{1.33}$ .<sup>23</sup> Similar to the EXAFS results, the Ga-Ti interactions were preferred; however, for the 1:3 and 1:2 ratio of Ga:Ti, the second shell Ga-M interactions include one and two pairs of Ga-Ga, respectively.

As shown in Table 2, the bond distance of Ga-O is almost unchanged with the change in Ga:Ti ratio. However, the Ga-Ti distance in the second and third shell increases with the decrease in Ga:Ti ratio. Compared to the 1:2 ratio of Ga:Ti, Ga-Ti distance in the second shell increases by 0.30% and 0.80% for the 1:3 and 1:5 ratio of Ga:Ti, and Ga-Ti separation in the third shell increases by 0.06% and 0.57%. The increased Ga-Ti distances, coupled with the unchanged Ga-O bond distances are indicative of an expansion in the Ti-O octahedral framework.

Another notable change is the Debye-Waller factor ( $\sigma^2$ ) which accounts for the variation in path length due to thermal and structural disorder in the material. Since all data were collected at the same temperature, the largest Debye-Waller factor of Ga-O bonds and that of Ga-Ti separations in the second shell (exhibited in the 1:5 ratio of Ga:Ti) must arise from structural disorder. This suggests that the least symmetric local structure occurs in the 1:5 ratio of Ga:Ti where large variations in the Ga-O and Ga-Ti distances are observed. Therefore, the increased concentration of Ti in the 1:5 ratio of Ga:Ti results in a more disordered local structure around Ga. Furthermore, recent DFT results show that for the 1:5 ratio of Ga:Ti, the energy difference between the lowest energy B-site configuration and the next lowest energy B-site configuration is only 0.012 eV, while the energy difference for the 1:3 ratio of Ga:Ti is 0.092 eV and for the 1:2 ratio of Ga:Ti is 0.222 eV.<sup>23</sup> The lower energy difference for the composition with the highest Cs loading represented by 1:5 ratio of Ga:Ti indicates less energetic favorability for any set of B-site configurations; hence, greater likelihood for disorder.

**TABLE 2** The best fitting results of Ga K edge data for three Ga-doped hollandite phases with Ga:Ti ratios of 1:2, 1:3, and 1:5

	Ga:Ti 1:2	Ga:Ti 1:3	Ga:Ti 1:5
First shell (Ga–O)			
Coordination ;number	6	6	6
Bond distance ;(Å)	1.972 ± 0.013	1.972 ± 0.007	1.972 ± 0.008
Distance from ;DFT results <sup>23</sup>	2.016	2.052	2.028
Debye–Waller ;factors (Å <sup>2</sup> )	0.0074 ± 0.0011	0.0068 ± 0.0007	0.0081 ± 0.0008
Second shell (Ga–Ga/Ti)			
Coordination ;number	4	4	4
Distance (Å)	3.014 ± 0.018	3.023 ± 0.011	3.038 ± 0.018
Distance from ;DFT results <sup>23</sup>	3.036	3.052	3.061
Debye–Waller ;factors (Å <sup>2</sup> )	0.0056 ± 0.0010	0.0057 ± 0.0008	0.0093 ± 0.0011
Third shell (Ga–Ga/Ti)			
Coordination ;number	4	4	4
Distance (Å)	3.484 ± 0.037	3.486 ± 0.022	3.504 ± 0.021
Distance from ;DFT results <sup>23</sup>	3.516	3.536	3.553
Debye–Waller ;factors (Å <sup>2</sup> )	0.0074 ± 0.0020	0.0071 ± 0.0013	0.0072 ± 0.0012

The best fit value for the  $S_0^2$  was found to be  $0.83 \pm 0.05$ .

**TABLE 3** Enthalpies of drop solution ( $\Delta H_{ds}$ ) in sodium molybdate solvent at 702°C and enthalpies of formation from constituent oxides ( $\Delta H_{f,ox}$ ) and from the elements ( $\Delta H_{f,el}$ ) of three hollandite phases at 25°C

Phase	$\Delta H_{ds}$ (kJ/mol)	$\Delta H_{f,ox}$ -EDS (kJ/mol)	$\Delta H_{f,ox}$ -ICP (kJ/mol)	$\Delta H_{f,el}$ -EDS (kJ/mol)	$\Delta H_{f,el}$ -ICP (kJ/mol)
Ba <sub>1.33</sub> Ga <sub>2.67</sub>	398.50 ± 5.90 (8)	−132.90 ± 7.55	−141.15 ± 7.61	−7338.59 ± 9.07	−7355.52 ± 9.14
(BaCs) <sub>0.667</sub> Ga <sub>2</sub>	435.34 ± 3.06 (8)	−159.49 ± 4.12	−157.45 ± 4.20	−7385.45 ± 6.47	−7387.66 ± 6.53
Cs <sub>1.33</sub> Ga <sub>1.33</sub>	470.66 ± 3.35 (8)	−206.55 ± 3.77	−179.35 ± 3.75	−7457.54 ± 6.58	−7431.04 ± 6.56

Uncertainty is two standard deviation of the mean and value in parentheses is the number of experiments.

### 3.3 | Thermochemistry

Atomic scale structural properties of hollandite are linked to thermodynamic properties through trends in calorimetric measurements. The drop solution enthalpies ( $\Delta H_{ds}$ ) of three hollandite phases measured in the molten sodium molybdate (3Na<sub>2</sub>O 4MoO<sub>3</sub>) solvent at 702°C are listed in Table 3. Using these values and previously reported  $\Delta H_{ds}$  and  $\Delta H_{f,el}$  (the enthalpies of formation from elements) data for BaO, Cs<sub>2</sub>O, Ga<sub>2</sub>O<sub>3</sub>, and TiO<sub>2</sub> (shown in Table 4), the enthalpies of formation at 25°C from the corresponding constituent oxides ( $\Delta H_{f,ox}$ ) and from elements ( $\Delta H_{f,el}$ ) were calculated using thermochemical cycles (eg, those for (BaCs)<sub>0.667</sub>Ga<sub>2</sub> with actual EDS composition are shown in Table 5).<sup>31–36</sup> As shown in Table 3 and Figure 5, the values of  $\Delta H_{f,ox}$  of the three Ga-doped hollandite phases are all exothermic, indicating that they are thermodynamically stable relative to their constituent oxides. Moreover, the  $\Delta H_{f,ox}$  values become increasingly exothermic as Cs content increases. In other words, the hollandite phase with

**TABLE 4** Enthalpies of drop solution in sodium molybdate solvent at 702°C ( $\Delta H_{ds}$ ) and enthalpies of formation from the elements ( $\Delta H_{f,el}$ ) at 25°C of related component binary oxides

Oxide	$\Delta H_{ds}$ (kJ/mol)	$\Delta H_{f,el}$ (kJ/mol)
BaO	−184.61 ± 3.21 (31)	−548.1 ± 2.1 (35)
Cs <sub>2</sub> O	−348.9 ± 1.7 (32)	−346.0 ± 1.2 (35)
Ga <sub>2</sub> O <sub>3</sub>	130.16 ± 1.66 (33)	−1089.1 (36)
TiO <sub>2</sub>	60.81 ± 0.11 (34)	−944.0 ± 0.8 (35)

higher Cs content is more thermodynamically stable, which agrees with the trend calculated by our previous DFT calculations.<sup>23</sup> The driving force for the increase in energetic stability with increased Cs content comes from two main sources. The first is the strongly basic character of Cs<sub>2</sub>O, which makes ternary compound formation with relatively acidic oxides very exothermic. The second is enhanced capacity for disorder in the octahedral framework observed for the 1:5 ratio of Ga:Ti with increased Cs content as described in the previous section.

**TABLE 5** Thermochemical cycles used for calculation of enthalpies formation of targeted  $(\text{BaCs})_{0.667}\text{Ga}_2$  hollandite from constituent oxides ( $\Delta H_{f,\text{ox}}$ ) and from the elements ( $\Delta H_{f,\text{el}}$ ) at 25°C with correction based on EDS analyzed composition in Table 1

Enthalpy of formation of $\text{Ba}_{0.62}\text{Cs}_{0.62}\text{Ga}_{2.05}\text{Ti}_6\text{O}_{16}$ from the oxides at 25°C ( $\Delta H_{f,\text{ox}}$ )	
$\text{Ba}_{0.62}\text{Cs}_{0.62}\text{Ga}_{2.05}\text{Ti}_6\text{O}_{16}$ (s,25°C) $\rightarrow$ 0.62 BaO (sln,702°C) + 0.31 Cs <sub>2</sub> O (sln,702°C) + 1.025 Ga <sub>2</sub> O <sub>3</sub> (sln,702°C) + 6 TiO <sub>2</sub> (sln,702°C)	$\Delta H_{\text{ds}}$
0.62 BaO (s,25°C) $\rightarrow$ 0.62 BaO (sln,702°C)	$\Delta H_1$
0.31 Cs <sub>2</sub> O (s,25°C) $\rightarrow$ 0.31 Cs <sub>2</sub> O (sln,702°C)	$\Delta H_2$
1.025 Ga <sub>2</sub> O <sub>3</sub> (s,25°C) $\rightarrow$ 1.025 Ga <sub>2</sub> O <sub>3</sub> (sln,702°C)	$\Delta H_3$
6 TiO <sub>2</sub> (s,25°C) $\rightarrow$ 6 TiO <sub>2</sub> (sln,702°C)	$\Delta H_4$
0.62 BaO (s,25°C) + 0.31 Cs <sub>2</sub> O (s,25°C) + 1.025 Ga <sub>2</sub> O <sub>3</sub> (s,25°C) + 6 TiO <sub>2</sub> (s,25°C) $\rightarrow$ $\text{Ba}_{0.62}\text{Cs}_{0.62}\text{Ga}_{2.05}\text{Ti}_6\text{O}_{16}$ (s,25°C)	$\Delta H_{f,\text{ox}}$
$\Delta H_{f,\text{ox}} = \sum \Delta H_i$ (i = 1-4) - $\Delta H_{\text{ds}}$	
Enthalpy of formation of $\text{Ba}_{0.62}\text{Cs}_{0.62}\text{Ga}_{2.05}\text{Ti}_6\text{O}_{16}$ from the elements at 25 °C ( $\Delta H_{f,\text{el}}$ )	
0.62 BaO (s,25°C) + 0.31 Cs <sub>2</sub> O (s,25°C) + 1.025 Ga <sub>2</sub> O <sub>3</sub> (s,25°C) + 6 TiO <sub>2</sub> (s,25°C) $\rightarrow$ $\text{Ba}_{0.62}\text{Cs}_{0.62}\text{Ga}_{2.05}\text{Ti}_6\text{O}_{16}$ (s,25°C)	$\Delta H_{f,\text{ox}}$
0.62 Ba (s,25°C) + 0.31 O <sub>2</sub> (g,25°C) $\rightarrow$ 0.62 BaO (s,702°C)	$\Delta H_5$
0.62 Cs (s,25°C) + 0.155 O <sub>2</sub> (g,25°C) $\rightarrow$ 0.31 Cs <sub>2</sub> O (s,702°C)	$\Delta H_6$
2.05 Ga (s,25°C) + 1.5375 O <sub>2</sub> (g,25°C) $\rightarrow$ 1.025 Ga <sub>2</sub> O <sub>3</sub> (s,702°C)	$\Delta H_7$
6 Ti (s,25°C) + 6 O <sub>2</sub> (g,25°C) $\rightarrow$ 6 TiO <sub>2</sub> (s,702°C)	$\Delta H_8$
0.62 Ba (s,25°C) + 0.62 Cs (s,25°C) + 2.05 Ga (s,25°C) + 6 Ti (s,25°C) + 8 O <sub>2</sub> (g,25°C) $\rightarrow$ $\text{Ba}_{0.62}\text{Cs}_{0.62}\text{Ga}_{2.05}\text{Ti}_6\text{O}_{16}$ (s,25°C)	$\Delta H_{f,\text{el}}$
$\Delta H_{f,\text{el}} = \Delta H_{f,\text{ox}} + \sum \Delta H_i$ (i = 5-8)	

Large exothermic formation enthalpies of the three Ga-doped hollandites indicate that they are very stable relative to their binary constituent oxides, but one must also consider their stability with respect to other competing phase assemblages including ternary constituent oxides when evaluating their suitability as nuclear waste forms.<sup>20,37</sup> A

not been reported in SYNROC systems and are not considered further in this analysis.<sup>37</sup> In addition, enthalpies of formation are not available for many of these potential phases and will not be considered in the subsequent analysis.

The enthalpies of reaction ( $\Delta H_{\text{rxn}}$ ) at standard conditions are calculated as follows:<sup>20,37</sup>

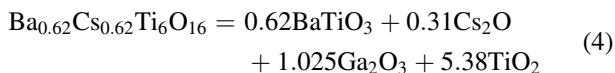
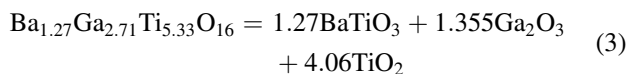
$$\Delta H_{\text{rxn},(\text{Ba}1.33\text{Ga}2.67\text{-EDS})} = 1.27\Delta H_{f,\text{ox}}(\text{BaTiO}_3) - \Delta H_{f,\text{ox}}(\text{Ba}1.33\text{Ga}2.67\text{-EDS}) = -60.52 \pm 9.10 \text{ kJ/mol}$$

$$\Delta H_{\text{rxn},(\text{Ba}1.33\text{Ga}2.67\text{-ICP})} = 1.31\Delta H_{f,\text{ox}}(\text{BaTiO}_3) - \Delta H_{f,\text{ox}}(\text{Ba}1.33\text{Ga}2.67\text{-ICP}) = -66.61 \pm 9.24 \text{ kJ/mol}$$

$$\Delta H_{\text{rxn},((\text{BaCs})0.667\text{Ga}2\text{-EDS})} = 0.62\Delta H_{f,\text{ox}}(\text{BaTiO}_3) - \Delta H_{f,\text{ox}}((\text{BaCs})0.667\text{Ga}2\text{-EDS}) = 65.06 \pm 4.81 \text{ kJ/mol}$$

$$\Delta H_{\text{rxn},((\text{BaCs})0.667\text{Ga}2\text{-ICP})} = 0.67\Delta H_{f,\text{ox}}(\text{BaTiO}_3) - \Delta H_{f,\text{ox}}((\text{BaCs})0.667\text{Ga}2\text{-ICP}) = 55.41 \pm 4.98 \text{ kJ/mol}$$

conceivable phase assemblage may contain BaTiO<sub>3</sub> (perovskite) and other constituent oxides, which can be assessed by thermodynamics using the following reactions outlined in Equations 3 and 4 (actual EDS stoichiometries are used as examples):<sup>20,37</sup>



Cs–Ga–O, Cs–Ti–O, Ba–Ga–O, and Ga–Ti–O type phases are theoretically potential phases, however they have

where  $\Delta H_{f,\text{ox}}$  values of hollandite are from Table 3,  $\Delta H_{f,\text{ox}}(\text{BaTiO}_3) = -152.3 \pm 4.0 \text{ kJ/mol}$ .<sup>38</sup>

From  $\Delta H_{\text{rxn}}$  of three hollandites obtained above, it can be concluded that  $(\text{BaCs})_{0.667}\text{Ga}_2$  is energetically stable at room temperature with respect to BaTiO<sub>3</sub>, Cs<sub>2</sub>O, Ga<sub>2</sub>O<sub>3</sub>, and TiO<sub>2</sub>, as its  $\Delta H_{\text{rxn}}$  is endothermic. In contrast, the pure barium substituted end member  $\text{Ba}_{1.33}\text{Ga}_{2.67}$  is not stable with respect to BaTiO<sub>3</sub>, Ga<sub>2</sub>O<sub>3</sub>, and TiO<sub>2</sub>, as determined by the exothermic  $\Delta H_{\text{rxn}}$ . These estimates provide further evidence that increased Cs substitution stabilizes the hollandite phase from the perspective of formation enthalpy of the targeted phase, as well as from possible decomposition to other phases.

### 3.4 | Durability

The samples utilized for leaching tests were prepared from a different batch from the samples used for EXAFS and calorimetry described in previous sections, however their crystal structures and compositions have been verified and detailed processing parameters can be found in a previous publication<sup>12</sup> The leaching tests were conducted as a method to compare the relative leach resistance of Ga-doped hollandite samples. Three replicates were prepared for each sample with a constant 1:10 ratio of sample mass (M) to volume (V) of leachate. Although 1.5 g of -100/+200 mesh sample with 15 mL of water was targeted, sufficient quantities of material of the target mesh size could not be produced given the limited amount of sample combined with the grinding behavior. In the event, materials were collected from a smaller sieve fraction (-200/+270) to complete the three replicates. Each replicate consisted of a single sieve fraction particle size (ie, -100/+200 or -200/+270). The experimental constraints yielded replicates with different surface area to volume ratios (SA/V), which were used to normalize the leach results. Additional experimental data are summarized in Table S1.<sup>§</sup>

The three replicates of normalized Cs and Ga release for each composition are shown in Figure 6A,B, respectively. In general, for a given composition the replicates of elemental release, normalized to surface area, are in good agreement. However, one replicate from the  $\text{Ba}_{1.04}\text{Cs}_{0.24}\text{Ga}_{2.32}$  sample and one replicate from the  $\text{Ba}_{1.33}\text{Ga}_{2.67}$  sample appear to be outliers. No commonality to distinguish the behavior of those replicates could be determined. Instead, these outliers may represent the variability in crystalline systems and suggests the importance of sample preparation on the PCT results.<sup>¶</sup> Additionally, these samples correspond to the samples with the lowest Cs content which have the least favorable formation enthalpy and may be susceptible to some microstructure variation owing to less homogeneous phase formation. Nevertheless, these data do not significantly change the observed trend in Cs or Ga release shown in Figure 6A,B.

The measured normalized Cs release was relatively low in the  $(\text{BaCs})_{0.667}\text{Ga}_2$  and  $\text{Cs}_{1.33}\text{Ga}_{1.33}$  samples compared to that of the  $\text{Ba}_{1.04}\text{Cs}_{0.24}\text{Ga}_{2.32}$  sample. Similarly, the measured normalized Ga release was relatively low in the samples with higher concentrations of Cs substitution

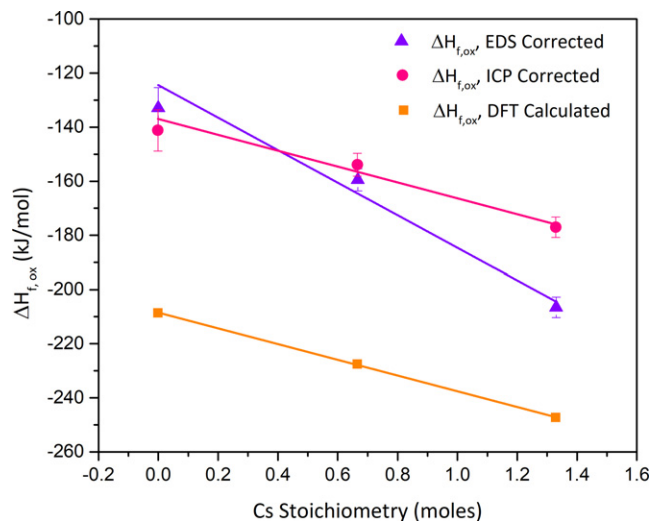


**FIGURE 5** The trends of values of experimental and DFT calculated enthalpies of formation from the constituent oxides at 25°C ( $\Delta H_{f,ox}$ ) for all three Ga-doped hollandite phases as  $\text{Ba}_{1.33}\text{Ga}_{2.67}$ ,  $(\text{BaCs})_{0.667}\text{Ga}_2$  and  $\text{Cs}_{1.33}\text{Ga}_{1.33}$

compared to the  $\text{Ba}_{1.33}\text{Ga}_{2.67}$  sample which showed a marked increase in Ga release. For both elements, a minimum in elemental (Cs and Ga) release was measured in the  $(\text{BaCs})_{0.667}\text{Ga}_2$  sample. Consequently, results of the leaching tests suggest that elemental (Cs and Ga) release decreases with increasing Cs concentration in Ga-doped hollandites. The decrease may be gradual or there may be a threshold Cs concentration at which the elemental release significantly decreases. The leachate analysis, when compared to atomistic level structural features and the calorimetry data, not only indicates a correlation between thermodynamic stability and elemental release, but also suggests a more complex relationship. Nevertheless, the combined atomistic level structural trends, calorimetry and leachate results, generally agree and provide evidence, for the first time, that elemental release is related to the thermodynamic stability in these Ga-doped hollandite systems. This study also suggests that compositional screening based on formation enthalpies should be used as materials design criteria for waste form development.

## 4 | CONCLUSIONS

A series of Ga-doped titanate hollandite phases were studied across the A-site solid solution. The experimentally measured enthalpies of formation were found to be more negative and hence more favorable with increased Cs content in agreement with recent computational predictions.<sup>23</sup> At the atomistic level, this was related to the local structure around the Ga and Ti on B-sites. Finally, aqueous leaching

<sup>§</sup>The PCT methodology (ie, Method B) does not assure direct comparison to other samples unless identical test protocols (eg, sample surface area, particle morphology, water volume, etc.) are maintained and if the dissolution mechanisms are similar.<sup>27</sup>

<sup>¶</sup>Owing to less-than ideal usable material after grinding, sieving, and washing steps for the PCT, 1-g samples were used for these replicates. One gram is acceptable as the lower limit in the standard PCT procedure.

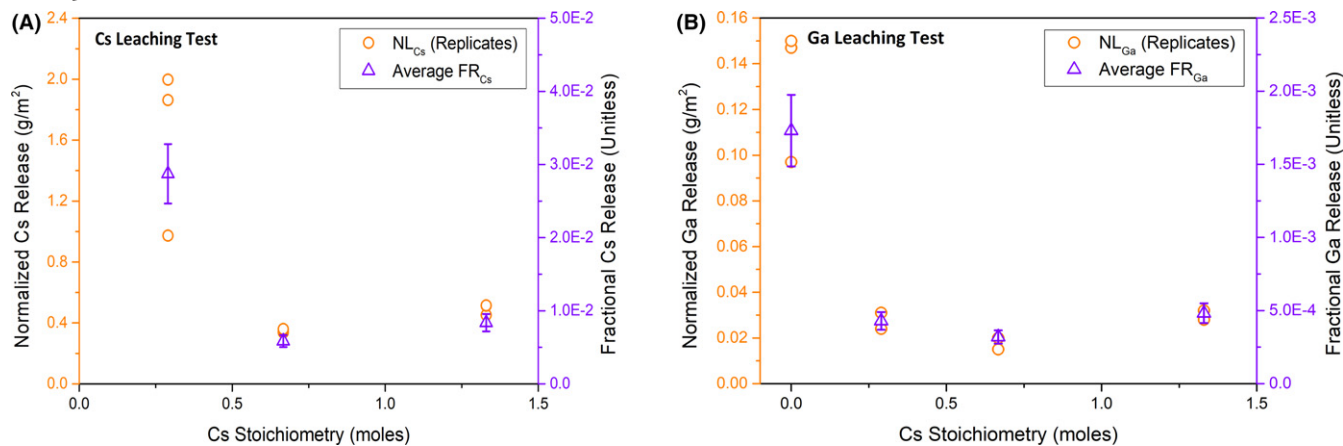


**FIGURE 6** Normalized elemental release ( $NL_i$ ,  $\text{g/m}^2$ ) and the computed fractional elemental release ( $FR_i$ , unitless) of (A) Cs and (B) Ga for different sintered Ga-doped hollandite phases incorporating different Cs contents. Error bars of average fractional elemental release stand for standard deviations

tests revealed that high Cs content hollandite phases exhibited greater Cs retention as compared to low Cs content hollandite. While preliminary in nature, this work draws attention to the links between the capacity for radionuclide retention, atomistic level structural features and bulk thermodynamic properties of materials.

## ACKNOWLEDGMENTS

KSB, YX, and LSN gratefully acknowledge financial support from the DOE-EPSCoR Project Number: DE-SC0012530, “Radionuclide Waste Disposal: Development of Multi-scale Experimental and Modeling Capabilities” for support of modelling and EXAFS studies. KSB and MZ acknowledge support of thermodynamic measurements as part of the Center for Hierarchical Waste Form Materials, an Energy Frontier Research Center funded by the U.S. Department of Energy, Office of Science, Basic Energy Sciences under Award No. DE-SC0016574. AIF and YL acknowledge support of EXAFS data analysis by the U.S. Department of Energy, Office of Basic Energy Sciences under Grant No. DE-FG02-03ER15476. The calorimetric experiments carried out at University of California, Davis were supported as part of the Materials Science of Actinides, an Energy Frontier Research Center funded by the U.S. Department of Energy, Office of Science, Basic Energy Sciences under Award Number DE-SC0001089. JA acknowledges the support of durability testing by the U.S. Department of Energy, Office of Nuclear Energy, Fuel Cycle Technology, Materials Recovery and Waste Form Development Campaign. Work conducted at Savannah River National Laboratory was supported by the U.S. Department of Energy under contract number DE-AC09-08SR22470.

## CONFLICT OF INTEREST

The authors declare no competing financial interest.

## ORCID

Alexandra Navrotsky  <https://orcid.org/0000-0002-3260-0364>

Kyle S. Brinkman  <https://orcid.org/0000-0002-2219-1253>

## REFERENCES

1. Ewing RC. Long-term storage of spent nuclear fuel. *Nat Mater.* 2015;14(3):252.
2. Hamilton LH, Scowcroft B, Ayers MH, Bailey VA, Carnesale A, Domenici PV, et al. *Blue ribbon commission on America's nuclear future: report to the secretary of energy.* Washington, DC: US Department of Energy. 2012.
3. Lee WE, Ojovan MI, Stennett MC, Hyatt NC. Immobilisation of radioactive waste in glasses, glass composite materials and ceramics. *Adv Appl Ceram.* 2006;105(1):3–12.
4. Crum J, Maio V, McCloy J, Scott C, Riley B, Benefiel B, et al. Cold crucible induction melter studies for making glass ceramic waste forms: a feasibility assessment. *J Nucl Mater.* 2014;444(1–3):481–92.
5. Amoroso JW, Marra J, Dandeneau CS, Brinkman K, Xu Y, Tang M, et al. Cold crucible induction melter test for crystalline ceramic waste form fabrication: a feasibility assessment. *J Nucl Mater.* 2017;486:283–97.
6. McCarthy GJ. High-level waste ceramics: materials considerations, process simulation, and product characterization. *Nucl Technol.* 1977;32(1):92–105.
7. Roy R. Rational molecular engineering of ceramic materials. *J Am Ceram Soc.* 1977;60(7–8):350–63.
8. McCarthy GJ. High-level waste ceramics. *Trans Am Nucl Soc.* 1976;23:168–9.

9. Ringwood A, Kesson SE, Ware NG, Hibberson W, Major A. Immobilisation of high level nuclear reactor wastes in SYNROC. *Nature*. 1979;278(5701):219.
10. Aubin-Chevaldonnet V, Caurant D, Dannoux A, Gourier D, Charpentier T, Mazerolles L, et al. Preparation and characterization of (Ba, Cs)(M, Ti) 8O16 (M= Al<sup>3+</sup>, Fe<sup>3+</sup>, Ga<sup>3+</sup>, Cr<sup>3+</sup>, Sc<sup>3+</sup>, Mg<sup>2+</sup>) hollandite ceramics developed for radioactive cesium immobilization. *J Nucl Mater*. 2007;366(1–2):137–60.
11. Michiue Y, Sato A, Watanabe M. Low-temperature phase of sodium priderite, Na<sub>x</sub>Cr<sub>x</sub>Ti<sub>8-x</sub>O<sub>16</sub>, with a monoclinic hollandite structure. *J Solid State Chem*. 1999;145(1):182–5.
12. Xu Y, Wen Y, Grote R, Amoroso J, Nickles LS, Brinkman KS. A-site compositional effects in Ga-doped hollandite materials of the form Ba<sub>x</sub>Cs<sub>y</sub>Ga<sub>2x+y</sub>Ti<sub>8-2x-y</sub>O<sub>16</sub>: implications for Cs immobilization in crystalline ceramic waste forms. *Sci Rep*. 2016;6:27412.
13. Sun W, Song Y, Gong XQ, Cao LM, Yang J. Hollandite structure K<sub>x</sub> ≈ 0.25 IrO<sub>2</sub> catalyst with highly efficient oxygen evolution reaction. *ACS Appl Mater Interfaces*. 2015;8(1):820–6.
14. Larson AM, Moetakef P, Gaskell K, Brown CM, King G, Rodriguez EE. Inducing ferrimagnetism in insulating hollandite Ba<sub>1.2</sub>Mn<sub>8</sub>O<sub>16</sub>. *Chem Mater*. 2015;27(2):515–25.
15. Huang J, Poyraz AS, Lee SY, Wu L, Zhu Y, Marschilok AC, et al. Silver-containing α-MnO<sub>2</sub> nanorods: electrochemistry in Na-based battery systems. *ACS Appl Mater Interfaces*. 2016;9(5):4333–42.
16. Huang J, Poyraz AS, Takeuchi KJ, Takeuchi ES, Marschilok AC. M x Mn 8 O 16 (M = Ag or K) as promising cathode materials for secondary Mg based batteries: the role of the cation M. *Chem Commun*. 2016;52(21):4088–91.
17. Das B, Reddy MV, Rao GS, Chowdari BV. Nano-phase tin hollandites, K<sub>2</sub>(M<sub>2</sub>Sn<sub>6</sub>)O<sub>16</sub>(M = Co, In) as anodes for Li-ion batteries. *J Mater Chem*. 2011;21(4):1171–80.
18. Brinkman K, Fox K, Marra J. *Crystalline ceramic waste forms: reference formulation report*. Aiken, SC: Savannah River Site; 2012.
19. Brinkman KS, Marra JC, Amoroso J, Tang M. *Crystalline ceramic waste forms: comparison of reference process for ceramic waste form fabrication*. Aiken, SC: Savannah River Site (SRS); 2013.
20. Costa GC, Xu H, Navrotsky A. Thermochemistry of barium hollandites. *J Am Ceram Soc*. 2013;96(5):1554–61.
21. Takahashi T, Kuwabara K. Ionic conductivities of hollandites. *Electrochim Acta*. 1978;23(4):375–9.
22. Barbato S, Gautier JL. Hollandite cathodes for lithium ion batteries. 2. Thermodynamic and kinetics studies of lithium insertion into BaMMn<sub>7</sub>O<sub>16</sub> (M = Mg, Mn, Fe, Ni). *Electrochim Acta*. 2001;46(18):2767–76.
23. Wen Y, Xu Y, Brinkman KS, Shuller-Nickles L. Atomistic scale investigation of cation ordering and phase stability in Cs-substituted Ba<sub>1.33</sub>Zn<sub>1.33</sub>Ti<sub>6.67</sub>O<sub>16</sub>, Ba<sub>1.33</sub>Ga<sub>2.66</sub>Ti<sub>5.67</sub>O<sub>16</sub> and Ba<sub>1.33</sub>Al<sub>2.66</sub>Ti<sub>5.33</sub>O<sub>16</sub> hollandite. *Sci Rep*. 2018;8(1):5003.
24. Ravel B, Newville MA. Athena, artemis, hephaestus: data analysis for X-ray absorption spectroscopy using IFEFFIT. *J Synchrotron Radiat*. 2005;12(4):537–41.
25. Navrotsky A. Progress and new directions in high temperature calorimetry revisited. *Phys Chem Miner*. 1997;24(3):222–41.
26. Navrotsky A. Progress and new directions in calorimetry: a 2014 perspective. *J Am Ceram Soc*. 2014;97(11):3349–59.
27. Jantzen C, Bibler N, Beam D. C1285–14 Standard test methods for determining chemical durability of nuclear, hazardous, and mixed waste glasses and multiphase glass ceramics: The product consistency test (PCT).
28. Amoroso J, Marra JC, Tang M, Lin Y, Chen F, Su D, et al. Melt processed multiphase ceramic waste forms for nuclear waste immobilization. *J Nucl Mater*. 2014;454(1):12–21.
29. Cocco AP, DeGostin MB, Wrubel JA, Damian PJ, Hong T, Xu Y, et al. Three-dimensional mapping of crystalline ceramic waste form materials. *J Am Ceram Soc*. 2017;100(8):3722–35.
30. Xu Y, Feyngenson M, Page K, Nickles LS, Brinkman KS. Structural evolution in hollandite solid solutions across the a-site compositional range from Ba<sub>1.33</sub>Ga<sub>2.66</sub>Ti<sub>5.34</sub>O<sub>16</sub> to Cs<sub>1.33</sub>Ga<sub>1.33</sub>Ti<sub>6.67</sub>O<sub>16</sub>. *J Am Ceram Soc*. 2016;99(12):4100–6.
31. Ushakov SV, Cheng J, Navrotsky A, Wu JR, Haile SM. Formation enthalpies of tetravalent lanthanide perovskites by high temperature oxide melt solution calorimetry. *MRS Online Proceedings Library Archive*. 2002;718:D7.17. <https://doi.org/10.1557/PROC-718-D7.17>
32. Ushakov SV, Navrotsky A, Farmer JM, Boatner LA. Thermochemistry of the alkali rare-earth double phosphates, A<sub>3</sub>RE(PO<sub>4</sub>)<sub>2</sub>. *J Mater Res*. 2004;19(7):2165–75.
33. Cheng J, Navrotsky A. Enthalpies of Formation of LaBO<sub>3</sub> Perovskites (B = Al, Ga, Sc, and In). *J Mater Res*. 2003;18(10):2501–8.
34. Putnam RL, Navrotsky A, Woodfield BF, Boerio-Goates J, Shapiro JL. Thermodynamics of formation for zirconolite (CaZrTi<sub>2</sub>O<sub>7</sub>) from T = 298.15 K to T = 1500 K. *J Chem Thermodyn*. 1999;31(2):229–43.
35. Robie RA, Hemingway BS. *Thermodynamic properties of minerals and related substances at 298.15 K and 1 bar (105 Pascals) pressure and at higher temperatures*. Reston, VA: US Government Printing Office; 1995.
36. Kerr JA, Lide DR. *CRC handbook of chemistry and physics 1999–2000: a ready-reference book of chemical and physical data*, vol. 9. Boca Raton, FL: CRC Press, 2000; p. 87.
37. Xu H, Wu L, Zhu J, Navrotsky A. Synthesis, characterization and thermochemistry of Cs-, Rb- and Sr-substituted barium aluminium titanate hollandites. *J Nucl Mater*. 2015;459:70–6.
38. Takayama-Muromachi E, Navrotsky A. Energetics of compounds (A<sub>2</sub>+ B<sub>4</sub>+ O<sub>3</sub>) with the perovskite structure. *J Solid State Chem*. 1988;72(2):244–56.

## SUPPORTING INFORMATION

Additional supporting information may be found online in the Supporting Information section at the end of the article.

**How to cite this article:** Zhao M, Xu Y, Shuller-Nickles L, et al. Compositional control of radionuclide retention in hollandite-based ceramic waste forms for Cs-immobilization. *J Am Ceram Soc*. 2018;00:1–11. <https://doi.org/10.1111/jace.16258>